1
Computational Insights into the Structural Properties and Catalytic Functions of Selenoprotein Glutathione Peroxidase (GPx)

Rajeev Prabhakar, Keiji Morokuma, and Djamaladdin G. Musaev

1.1
Introduction

Selenium (Se) was discovered in 1817, and in mammals its deficiency has been associated with many fatal diseases, such as cancer, HIV, cardiovascular and Keshan-Back [1, 2]. In most selenoproteins discovered so far, Se is present as a selenocysteine residue that plays an important role in the catalytic activities of these enzymes [3]. One of the first selenoproteins to be discovered was Glutathione Peroxidase (GPx), which demonstrated a strong anti-oxidant activity [4, 5]. This protein reduces numerous reactive oxygen species (ROS), including hydrogen peroxide [4] and peroxynitrite [6], by utilizing various reducing substrates, and protects cell membranes and other cellular components against oxidative damage [4].

Four different classes of Se-dependent GPx have been classified: (1) cytosolic (GPx-1), (2) gastrointestinal tract (GPx-2), (3) extracellular (GPx-3) and (4) phospholipid hydroperoxide (GPx-4) [3]. All four types are easily reduced by glutathione while they also accept some other reducing substrates. For example, GPx-3 can be reduced by glutaredoxin and thioredoxin [7], and GPx-4 utilizes protein thiols as reducing substrates [8, 9]. The catalytic activity of GPx has been mimicked in various organoselenium compounds possessing a direct Se–N bond; the most prominent among them is an anti-inflammatory drug called ebselen [10–12].

The only crystal structures elucidated are of bovine erythrocyte (intracellular enzyme, GPx-1) and human plasma (extracellular enzyme, GPx-3) GPx, resolved at 2.0 and 2.9 Å resolution, respectively [13, 14]. The complete X-ray structure of human plasma GPx (2.9 Å) is available in the literature [4]. These enzymes are tetrameric, with two asymmetric units containing two dimers that exhibit half-site reactivity. The dimeric X-ray structure is shown in Figure 1.1 and each monomer contains a critical selenocysteine residue. The following experimental observations explicitly implicate this residue in the catalytic cycle: (a) Treatment

Computational Modeling for Homogeneous and Enzymatic Catalysis.
A Knowledge-Base for Designing Efficient Catalysts. K. Morokuma and D. G. Musaev (Eds.)

ISBN: 978-3-527-31843-8

of the oxidized enzyme with cyanide destroys the catalytic activity and releases selenium from the enzyme [15]. (b) Iodoacetate inhibits only the substrate-reduced enzyme and reacts with the selenocysteine residue [16]. (c) A photoelectron spectroscopic study shows that the redox state of selenium in GPx depends on the substrate present [17]. (d) In the crystalline state the selenium sites of the oxidized enzyme can be reduced [18]. (e) The formation of E–Se–S–G complex through selenosulfide linkage has been demonstrated [19]. The overall active site structures of GPx-1 and GPx-3 enzymes are very similar, while the environments around their selenocysteine residue are quite different. Only half of the residues at the active site, within a range of 10 Å, are conserved in both enzymes [14].

As shown in Figure 1.1(C) at the active site the selenocysteine residue of the enzyme exists in the "resting" seleninic acid, E–Se(O)(OH), form. The active site residues Gln83 and Trp157 are located within hydrogen bonding distance of the selenium atom and have been suggested to play a critical role in the catalysis [13]. These two residues are conserved in the entire glutathione peroxidase superfamily and their homologues, which probably accounts for the similarities in

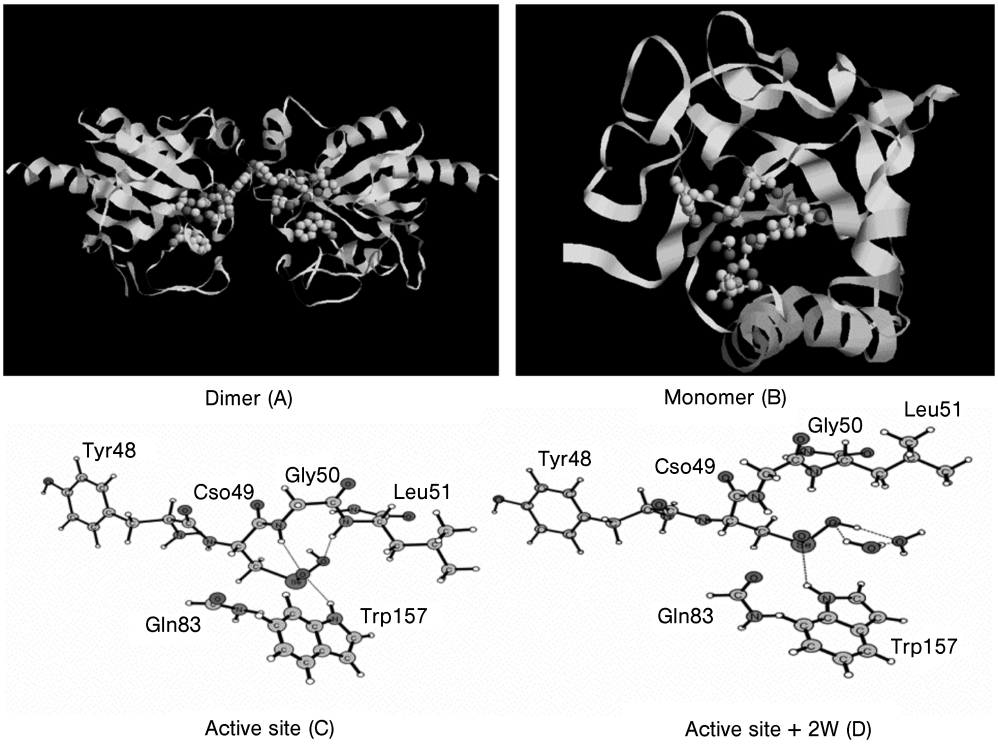

Figure 1.1 X-ray structures of (A) dimer, (B) monomer, (C) active site, and (D) optimized structure of the active site including two water molecules.

their catalytic mechanisms [20]. The active site seleninic acid residue is coordinated to Gly50 and Tyr48 in a tetradic arrangement [14]. The catalytically active form of GPx could either be as selenolate anion (E–Se^-) or selenol (E–SeH) [13].

1.2 Catalytic Functions

Based on substrate specificity the catalytic function of GPx enzyme is divided into two parts: (1) Peroxidase activity, and (2) Reductase activity.

1.2.1 Peroxidase Activity

GPx catalyzes the reduction of hydrogen peroxide, utilizing two molecules of glutathione. The proposed mechanism for the peroxidase activity is described by three elementary reactions (Figure 1.2). In the first step, Reaction (1), hydrogen peroxide reduction is accompanied by oxidation of the selenolate anion (or selenol) to selenenic acid. The experimentally measured rate for this reaction of 0.51 s^{-1} corresponds to a barrier of 14.9 kcal mol^{-1} [21]. In the second step, Reaction (2), the formed selenenic acid subsequently reacts with the substrate glutathione (GSH) to produce a seleno-sulfide adduct (E–Se–SG), which has been observed [19]. In the third step, Reaction (3), a second molecule of GSH attacks the seleno-sulfide adduct to regenerate the active form of the enzyme and form the disulfide (GS–SG). This step is suggested to be the rate-determining step of the entire mechanism [22]. Thus, in the full catalytic cycle, two equivalents of GSH are consumed to produce the disulfide and water.

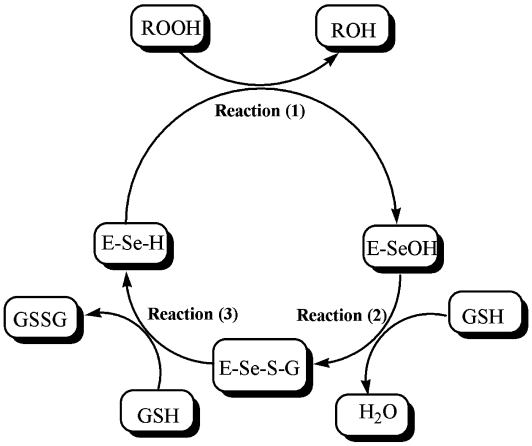

Figure 1.2 Experimentally suggested mechanism for the peroxidase activity of GPx.

1.2.2
Reductase Activity

Based on the extensive experimental [14, 23, 24] and theoretical [25] information for the peroxidase activity of GPx, the proposed catalytic mechanism for peroxynitrite/peroxynitrous acid ($ONOO^-$/ONOOH) reduction by this enzyme is shown in Figure 1.3. The suggested mechanism incorporates the fact that under physiological conditions the peroxynitrite reductase activity of GPx *in vivo* can follow either the ''oxidation'' or ''nitration'' of the critical selenocysteine residue [13, 24]. Therefore, these two processes are referred as ''oxidation'' and ''nitration'' pathways, respectively. As discussed below, only the first step, Reaction (1), of these pathways is completely different. In the ''oxidation'' pathway, $ONOO^-$/ONOOH reduction is accompanied by the oxidation of the selenol (E–SeH) to the selenenic acid (E–Se–OH), whereas in the ''nitration'' pathway the selenocysteine residue is nitrated by $ONOO^-$/ONOOH to generate E–Se–NO_2. For substrate $ONOO^-$, the experimentally measured rate for the formation of E–Se–OH expressed per monomer of reduced GPx of $2.0 \pm 0.2 \times 10^6$ M^{-1} s^{-1} corresponds to a barrier of 8.8 kcal mol^{-1} [23]. After the oxidation or nitration of the selenocysteine residue, the subsequent chemistry, Reactions (2) and (3) (Figure 1.2), in both pathways is similar. In the second step, Reaction (2), substrate glutathione (GSH) reacts with E–Se–OH or E–Se–NO_2 to produce seleno-sulfide adduct (E–Se–S–G). In Reaction (3), a second molecule of GSH attacks the seleno-sulfide adduct to regenerate the active form of the enzyme and form the disulfide (GS–SG).

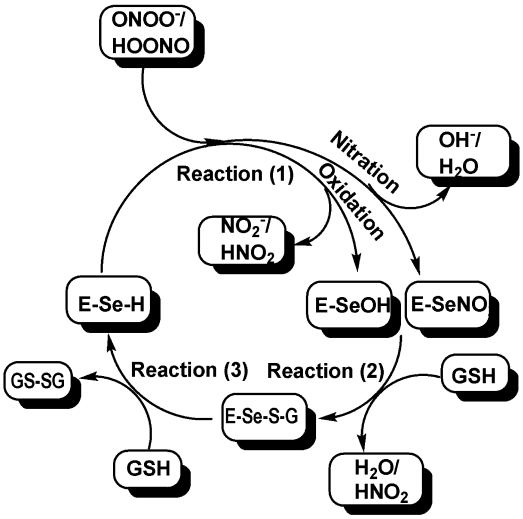

Figure 1.3 Experimentally suggested mechanism for the reductase activity of GPx.

Despite the availability of a great wealth of experimental information, the catalytic mechanism of GPx enzyme and the factors controlling its activity were not known with certainty. We have employed high-level quantum chemical approaches, namely pure quantum mechanics (QM) and hybrid quantum mechanics/molecular mechanics (QM/MM), incorporating all the available experimental information, to elucidate the catalytic mechanism of this interesting enzyme.

1.3 Computational Details

1.3.1 Computational Methods

All calculations were performed using the *Gaussian 03* program [26]. In the pure QM approach, the geometries of reactants, intermediates, transition states and products were optimized without any symmetry constraint using the B3LYP method [27] with the 6-31G(d) basis set. All degrees of freedom of proposed structures were optimized and frequency calculations were performed for all optimized minima and transition states. It was confirmed that the calculated minima have no imaginary frequency, while all transition states have one imaginary frequency corresponding to the reaction coordinate. The final energetics of the optimized structures were improved by performing single point calculations using a triple-zeta quality basis set 6-311+G(d,p). Since it was computationally not feasible to calculate zero-point energy and thermal corrections using the large basis set, these effects were estimated at the B3LYP/6-31G(d) level and added to the final B3LYP/6-311+G(d,p) energetics. This type of correction is an adequate approximation and has commonly been used in quantum chemical studies [28]. Dielectric effects from the surrounding environment were estimated using the self-consistent reaction field IEF-PCM method [29] at the B3LYP/6-31G(d) level. These calculations were performed with a dielectric constant of 4.3 corresponding to diethyl ether, close to 4.0 generally used to describe the protein surrounding. Throughout this chapter the energies obtained at the B3LYP/(6-311+G(d,p)) + zero-point energy (un-scaled) and thermal corrections (at 298.15 K and 1 atm) + solvent effects (the last three terms at B3LYP/6-31G(d) level) are used, while energies without the solvent effects are provided in parentheses.

The hybrid QM/MM approach allows the explicit inclusion of both steric and electrostatic effects from the protein surroundings. In this approach, the entire system (referred to as the "real system") is divided into two subsystems. The QM region (or model system) contains the active site, and is treated by quantum mechanics [B3LYP/6-31G)d level], and the MM region is treated at the MM level using the Amber force Field, and contains the rest of the protein. We used the two layer ONIOM(QM:MM) method [30, 31]. In this method, the interface between the QM region and the MM regions is treated by link atoms, and the interaction between the two layers is included at the classical level (mechanical embedding) [32].

1.3.2 Computational Models

Experimental studies on bovine erythrocyte GPx suggested a half-site reactivity of the enzyme [13], which justifies the use of the active site of only a monomer to investigate the enzyme reactivity. In the ''active site only'' approach, the first question to be considered is the choice of an appropriate model for the enzyme active site that retains all its basic features. Since the selenocysteine residue is, experimentally, suggested to play a critical role in the catalytic cycle, it is included in the model. The active site Gln83 and Trp157 residues, conserved in all known GPx's and experimentally suggested to be involved in the catalytic mechanism [13], are also included in the model. In addition, in the X-ray structure [13], the Tyr48, Gly50 and Leu51 residues form a part of the cage around the selenocysteine residue; therefore, they are also included in the model. Since the active site of GPx has been suggested to contain water molecules, a water molecule is also included in the active site model. Based on earlier experience, glutamine and tryptophan residues are modeled by formamide and indole, respectively. The substrate GSH (γ-glutamylcysteinylglycine, γ-GluCysGly) is a tri-peptide, which is modeled by ethanethiol (C_2H_5SH).

In the QM:MM approach, the entire monomer of GPx enzyme has been utilized as a model. In these studies, the aforementioned model of the active site forms the QM region, whereas the remaining part of the monomer constitutes the MM region. The overall system consists of 3113 atoms (86 in the QM region and 3027 in the MM region). Hydrogen atoms not included in the PDB-structure were added to the system, containing 196 amino acid residues, using the *GaussianView* program [33].

1.4 Results and Discussion

1.4.1 Refinement of the Active Site

The most notable difference between the active sites of GPx-1 and GPx-3 enzymes is the presence of two water molecules in the former, which, due to the low resolution of the X-ray structure, could not be observed in the latter. First, we explored the presence of water molecules at the active site of GPx-3 using the two-layer ONIOM (QM:MM) method [34]. In this study, the entire monomer (system **I**, Figure 1.1B) is chosen as a ''real'' system, extracted from the dimeric X-ray structure [4] (Figure 1.1A). The choice of monomeric unit is justified by the fact that in the crystal structure of the mammalian GPx (at 2.9 Å resolution) the active site selenocysteine residues are well separated, with an Se–Se distance of 23.2 Å.

Based on experimental information, the "active" part (Figure 1.1C) of the "real" system **I** includes SeCys, Tyr48, Gly50, Leu51, Gln83, and Trp157 residues. Later, system **I** was extended by adding two water molecules in the "active" part (Figure 1.1D) and called system **I(2W)**. All the structures belonging to the systems **I** and **I(2W)** are fully optimized at the Amber, ONIOM(HF/STO-3G:Amber)_ME and ONIOM(B3LYP/6-31G(d):Amber)_xx levels, where xx = ME or EE represents the mechanical embedding (ME) and the electronic embedding (EE) schemes.

Table 1.1 gives all the results, and comparisons have been made by the means of root-mean-square (RMS) deviations between the X-ray and optimized structures using only non-hydrogen atoms. The RMS deviations are 1.72, 1.71, and 1.71 Å between the X-ray and the Amber, ONIOM(HF/STO-3G:Amber)_ME and ONIOM(B3LYP/6-31G(d):Amber)_ME structures, respectively. Treatment of QM-MM interactions using the electronic embedding [ONIOM(B3LYP/6-31G(d):Amber)_EE] scheme gives an almost similar RMS deviation of 1.73 Å. These results indicate that irrespective of the method used the calculated RMS deviations remain the same and significant. The largest deviations between the calculated and X-ray structures correspond to the residues positioned near the second monomer, which should be improved with the inclusion of the second monomer into calculations. However, such large calculations were, technically, not feasible.

The RMS deviation of the critical active-site atoms is calculated to be 1.04 and 1.22 Å for the Amber and ONIOM(HF/STO-3G:Amber)_ME levels, respectively. Application of a higher-level method, ONIOM(B3LYP/6-31G(d):Amber)_ME, reduces it to 0.97 Å, which is still significant.

One major reason for such a significant deviation between the calculated and X-ray structure could be the low resolution (2.9 Å) of the X-ray structure. To corroborate the existence of water molecules at the active site of GPx-3 (2.9 Å), calculations have been performed that include two water molecules at the active site of system **I** from the X-ray structure of GPx-1 (2.0 Å). However, other possibilities, suggesting the presence of either one or more than two water molecules, can not be ruled out. As shown in Table 1.1, the inclusion of these two water molecules

Table 1.1 Calculated RMS deviations (in Å) for the monomer and the active site.

	Model	Monomer	Active site
X-ray – Amber	**I**	1.72	1.04
X-ray – ONIOM(HF:Amber)_ME	**I**	1.71	1.22
X-ray – ONIOM(B3LYP:Amber)_ME	**I**	1.71	0.97
X-ray – ONIOM(B3LYP:Amber)_EE	**I**	1.73	1.17
X-ray – ONIOM(B3LYP:Amber)_ME	**I(2W)**		0.79
X-ray – B3LYP	**I**, "active-site only"		2.26
X-ray – B3LYP	**I(2W)**, "active-site only"		1.48

[system **I(2W)**] indeed reduces the RMS deviation to 0.79 Å. This result suggests the existence of two bound water molecules at the active site of the mammalian GPx.

This conclusion is also supported by the ''active-site only'' calculations, which give a very large RMS deviation of 2.26 Å for the active site of system **I**. The inclusion of two water molecules into the ''active-site only'' system [active site of system **I(2W)**] reduces this deviation to 1.48 Å, which clearly indicates the importance of these two water molecules at the active site. However, notably, even the RMS deviation of 1.48 Å for the ''active-site only'' calculation of system **I(2W)** is still much larger than 0.79 Å obtained on including the protein environment. Thus this result explicitly demonstrates the significance of the protein–active-site interaction for the refinement of the active-site structure and, consequently, for the enzyme activity. Without excluding other possibilities, this study suggests that the active site of the 2.9 Å resolution X-ray structure needs to be complemented by two water molecules, which could be crucial for the catalytic activity of the enzyme.

1.4.2 Catalytic Functions: Peroxidase Activity

The catalytic cycle of the peroxidase activity of GPx can be described by the following overall reaction:

$$[\mathrm{E{-}SeH}](\mathrm{H_2O}) + \mathrm{HOOH} + 2\mathrm{RSH} \rightarrow [\mathrm{E{-}SeH}](\mathrm{H_2O})_2 + \mathrm{RS{-}SR} + \mathrm{H_2O}$$

As discussed above, this cycle consists of three elementary reactions and has been investigated at the B3LYP level [35]. In the first elementary reaction, $[\mathrm{E{-}SeH}] + \mathrm{H_2O_2} \rightarrow [\mathrm{E{-}SeOH}] + \mathrm{H_2O}$ (1), the active selenol [E–SeH] form of GPx takes up an hydrogen peroxide molecule and produces selenenic acid [E–SeOH] and a water molecule (Figure 1.4). The first step of Reaction (1) is the coordination of hydrogen peroxide molecule to the active site selenol [E–SeH] state of the enzyme to form a complex **II**. In **II**, the H_2O_2 molecule binds to the active site by forming strong hydrogen bonds with the water molecule and the Gly50 residue. This process is found to be exothermic by 6.3 (13.5) kcal mol^{-1}. From the complex **II**, the reaction is suggested to proceed via a stepwise pathway, which is divided into two parts: (a) proton transfer from [E–SeH] to the Gln83 residue through a hydrogen peroxide and a water molecule, leading to the formation of $[\mathrm{E{-}Se^-}]$ and protonated Gln83 (**III**), and (b) O–O bond cleavage via protonation of the terminal oxygen atom of H_2O_2 by the proton earlier transferred to Gln83 residue. As a result, a water molecule and selenenic acid (**IV**) are formed.

In the first part, the Se–H bond of the selenol $[\mathrm{R{-}Se^-}]$ is broken and, simultaneously, the proton is transferred through the oxygen atom of hydrogen peroxide and a water molecule to the neighboring Gln83, providing an intermediate product **III** (Figure 1.4). As a result, the selenolate anion $[\mathrm{R{-}Se^-}]$ and protonated Gln83 are formed. DFT calculations show that the first part of this stepwise path-

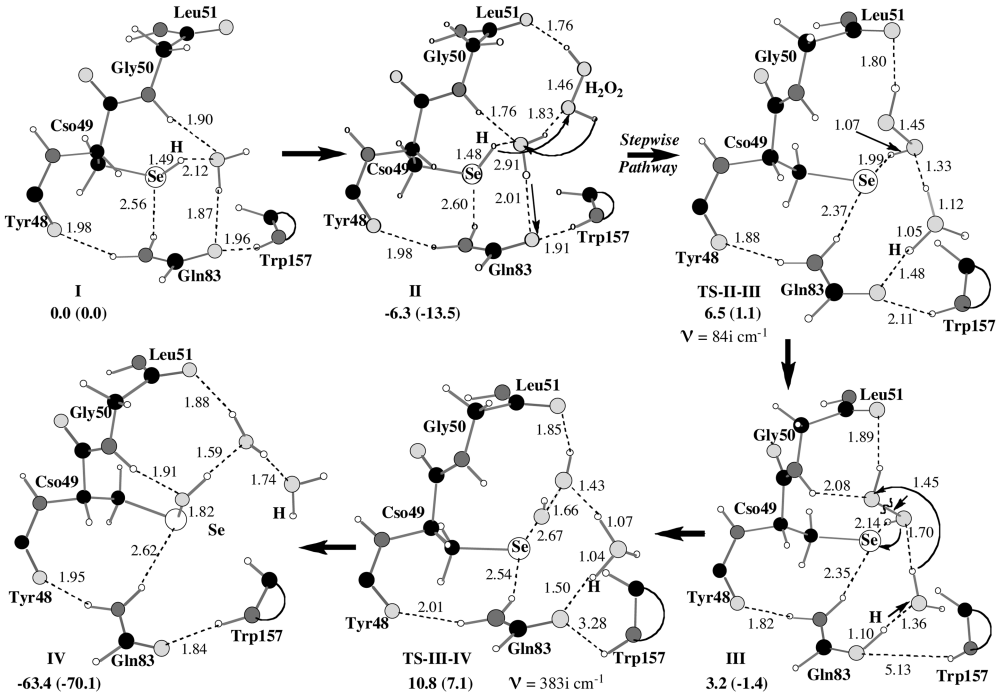

Figure 1.4 Optimized structures (in Å) and energies [with and without (in parenthesis) solvent effects, in kcal mol^{-1}] of reactant, intermediates and transition states for the stepwise mechanism of the reaction [E–SeH] + H_2O_2 → [E–SeOH] + H_2O (Reaction 1).

way occurs through transition state **TS-II-III** with a 12.8 (14.6) kcal mol^{-1} barrier and is endothermic by 9.5 (11.9) kcal mol^{-1}.

In the second part, the O–O bond of H_2O_2 is cleaved and the hydroxyl of H_2O_2 is transferred to the selenolate anion [E–Se$^-$]. In this part, the proton previously transferred to Gln83 residue moves to the terminal oxygen atom of H_2O_2 and cleaves the O–O bond, forming selenenic acid and a water molecule (**IV**). The barrier for this process is 7.6 (8.5) kcal mol^{-1}. Since the O–O bond cleavage is followed by the formation of **III**, which is endothermic by 9.5 (11.9) kcal mol^{-1}, the overall barrier for the formation of the selenenic acid [E–SeOH], Reaction (1), becomes 17.1 (20.6) kcal mol^{-1}. The calculated barrier for the hydrogen peroxide reduction is in excellent agreement with the experimentally measured barrier of 14.9 kcal mol^{-1} [21]. Reaction (1) is calculated to be exothermic by 63.4 (70.1) kcal mol^{-1}.

Based on the results obtained in the first part of this reaction, the Gln83 residue is suggested to play a key role of a proton acceptor, which is consistent with the experimental proposal indicating that the Gln83 residue participates in the catalytic cycle [13].

The second elementary reaction, [E–SeOH] + GSH → [E–Se–SG] + HOH (2), starts with the coordination of the first glutathione molecule to the previously formed selenenic acid [E–SeOH] to give a weak selenenic acid–glutathione complex (**V**) (Figure 1.5). The binding energy of [E–SeOH]–(GSH) is calculated to be 4.2 (7.5) kcal mol^{-1}. The reaction proceeds further through the transition state **TS-V-VI**, climbing a barrier of 17.9 (22.6) kcal mol^{-1}. In this process, synchronously, the S–H bond of the glutathione is broken and a proton is transferred to the hydroxyl group of the selenenic acid accompanied by the formation of a Se–S bond. In the product, the seleno-sulfide adduct (E–Se–SG) and a water molecule (**VI**) are formed. Reaction (2) is calculated to be exothermic by 15.9 (23.4) kcal mol^{-1}. Formation of E–Se–SG complex through selenosulfide linkage has been observed experimentally [19].

In the third and final elementary reaction, [E–Se–SG] + GSH → [E–SeH] + GS–SG (3),the second glutathione molecule (GSH), reacts with the seleno-sulfide adduct (**VI**) to produce the selenol [E–SeH] and oxidized disulfide (GS–SG) form of glutathione (**X**) (Figure 1.6).

We have explored several pathways for this reaction before suggesting the most plausible one. In this step, the S–H bond of the glutathione is broken and the proton is transferred via two water molecules to the amide backbone of Gly50. This process leads to the formation of the oxidized form of glutathione $C_2H_5S–SC_2H_5$ and protonated Gly50 residue. The amide backbone of Gly50 directly participates in this process and the presence of two water molecules is essential to bridge the proton donor (glutathione) and the acceptor (Gly50) sites. The calculated barrier for this step is 21.5 (25.5) kcal mol^{-1} and corresponds to the transition state **TS-VII-VIII**. This step is proposed to be a rate-determining step of the entire catalytic mechanism, which is in agreement with experiments

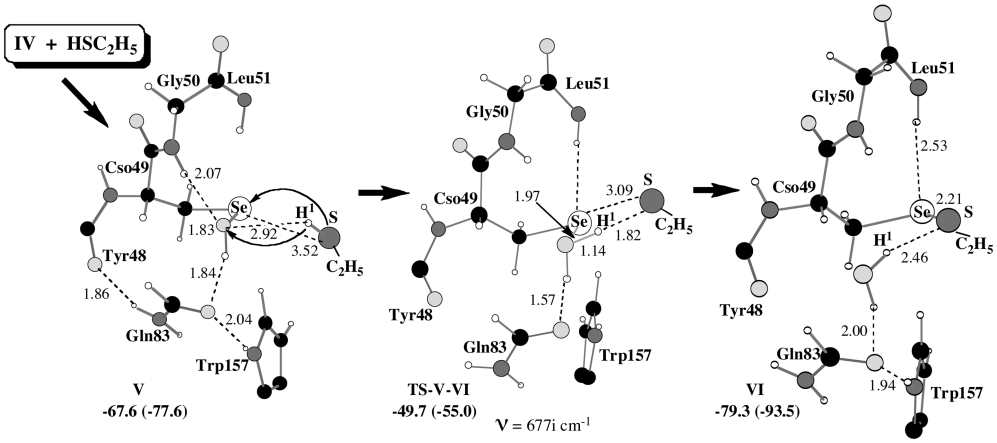

Figure 1.5 Optimized structures (in Å) and energies [with and without (in parenthesis) solvent effects, in kcal mol^{-1}] of reactant, intermediates and transition states for the reaction [E–SeOH] + GSH → [E–Se–SG] + HOH (Reaction 2).

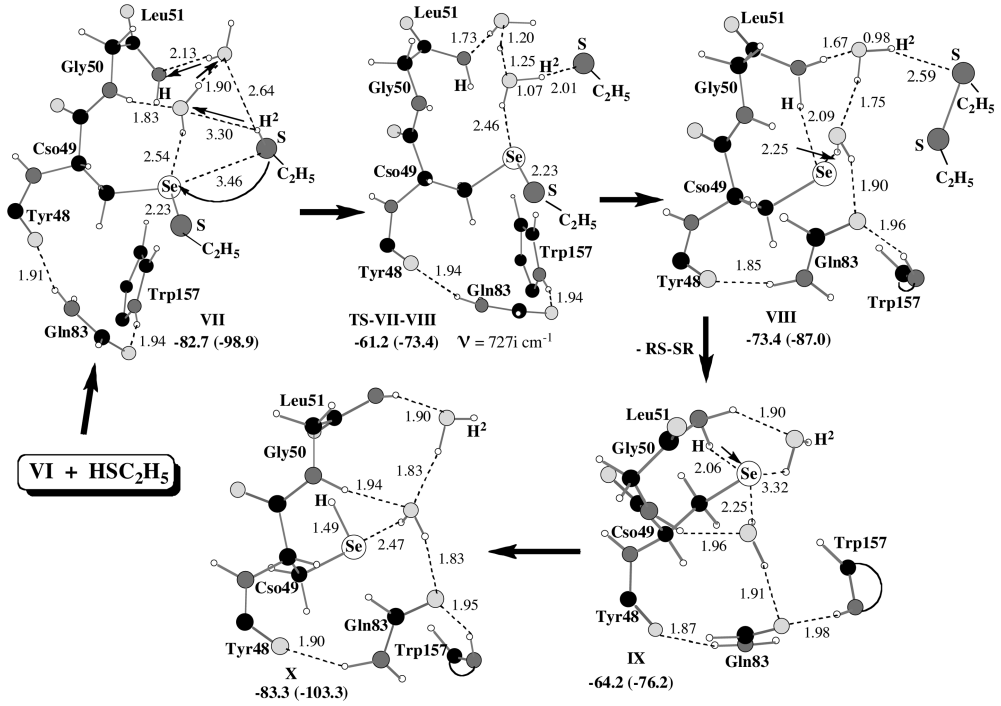

Figure 1.6 Optimized structures (in Å) and energies [with and without (in parenthesis) solvent effects, in kcal mol^{-1}] of reactant, intermediates and transition states for [E–Se–SG] + GSH → [E–SeH] + GS–SG (Reaction 3).

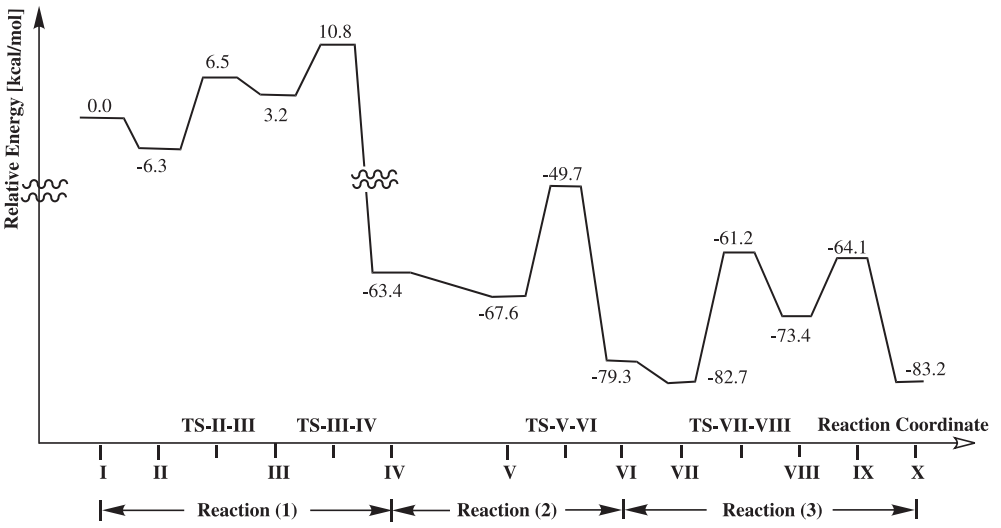

Figure 1.7 Energy diagram for the peroxidase activity of GPx (including solvent effects).

[22]. The product **VIII** formed in this step could be described as a weakly-bound complex where the selenocysteine residue is in its selenolate (E–Se^-) form. Later, this product rearranges to the final product of selenol **X**, with almost no barrier. Formation of the selenol (E–SeH) is exothermic by 19.1 (27.1) kcal mol^{-1} and the enzyme returns to its original form.

Figure 1.7 shows the energy diagram of the peroxidase activity of GPx.

1.4.3 Catalytic Functions: Effect of the Surrounding Protein on the Peroxidase Activity

To evaluate the quantitative effect of the protein surroundings on the energy we investigated the catalytic mechanism of hydrogen peroxide reduction by glutathione peroxidase (GPx) by including the complete protein environment in the calculations [35]. The two-layer ONIOM(QM:MM) method was employed to explore the potential energy surface (PES) of Reaction (1), $[E–SeH] + H_2O_2 \rightarrow [E–SeOH] + H_2O$ (1), in the catalytic cycle. Comparison of this PES with that reported in our previous ''active site only'' study allows us to assess the effect of the protein environment on the proposed mechanism. The most relevant results of the previous study are:

1. According to experimental data [13], the active state of the selenocysteine residue could be either the selenolate anion [E–Se^-] or selenol [E–SeH]. Our calculations showed that E–SeH is the most preferable active form of the enzyme [25].
2. From the X-ray structure [14], the geometry optimization led to two different conformers of Gln83 residue in the ''active site only'' model (either the oxo or the $–NH_2$ group of Gln83 facing Trp157), while Trp157 deviated significantly from its position in the X-ray structure.
3. In general, selenenic acid [E–SeOH] formation could occur either via a concerted or stepwise mechanism. Our calculations using the ''active site only'' models show that the barrier for the concerted mechanism is 4.2 kcal mol^{-1} higher than that for the stepwise mechanism [25].

In this ONIOM (QM:MM) study, the aforementioned theoretical conclusions from the previous study are fully utilized to investigate the reaction mechanism of H_2O_2 reduction catalyzed by GPx; here we only investigate the mechanisms identified as plausible in the ''active site only'' study.

1.4.3.1 Hydrogen Peroxide Coordination

The starting point of this study is the optimization of the structure of the enzyme. In contrast to the ''active site only'' study, the ONIOM calculations made in the presence of the surrounding protein yield only a single stable conformation of Gln83 (**I**, Figure 1.8). During optimization both Gln83 and Trp157 re-

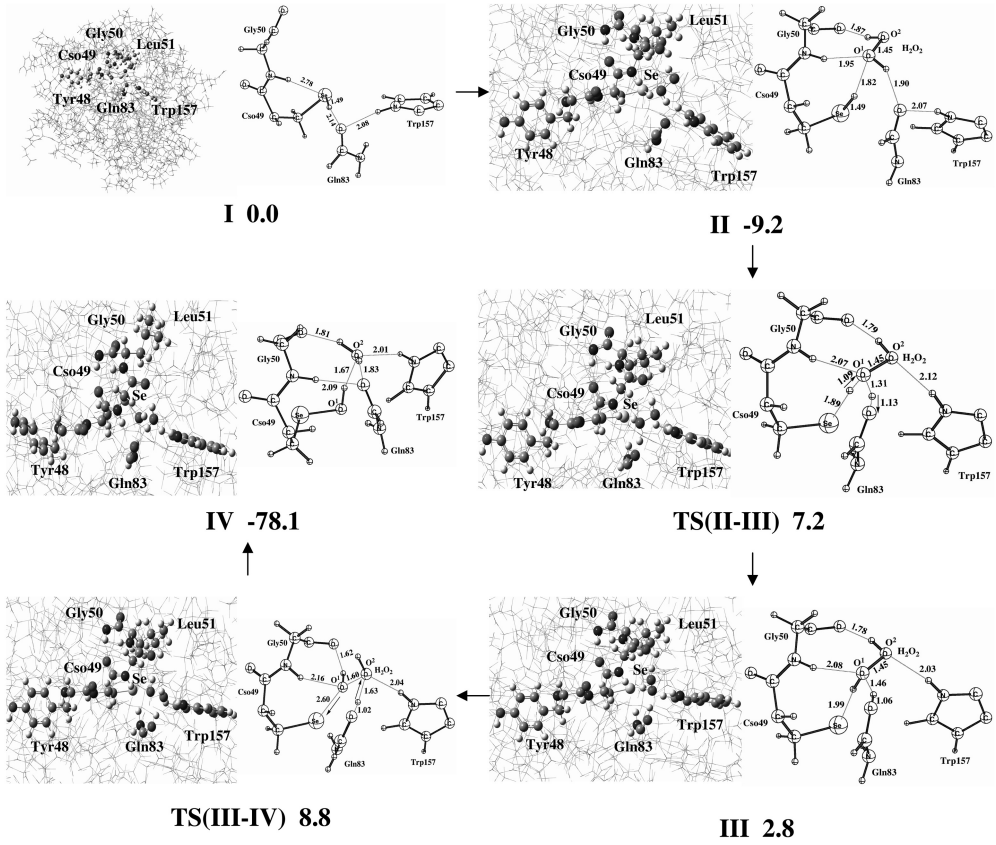

Figure 1.8 Optimized ONIOM structures (C atoms in gray, H atoms in white, and O and N atoms in black) with critical reaction coordinates (separately displayed in the adjoining views, in Å) and energies (kcal mol^{-1}) of reactant, intermediates and transition states and product for the H_2O_2 reduction mechanism of GPx.

sidues largely retained their positions shown in the X-ray structure. The effect of the protein environment on the structure of the active site is also reflected in the RMS deviations between the optimized and the X-ray structures, which are 1.48 and 0.97 Å for the ''active site only'' and QM/MM calculations, respectively.

In the first step of Reaction (1), similarly as for the ''active site only'' system, a hydrogen peroxide molecule coordinates to the active site of the enzyme to produce **II** (Figure 1.8). In **II**, H_2O_2 forms strong hydrogen bonds with Cso49, Gln83 and Gly50 residues, and has a binding energy of 9.2 (6.3) kcal mol^{-1}. In the presence of the protein environment the $SeH{-}O^1$ bond (1.82 Å) is shorter than the corresponding bond (1.91 Å) in the ''active site only'' system. As discussed above, in the present study we did not include a water molecule in the active site, which in the case of ''active site only'' investigations was shown to reduce the H_2O_2

binding energy by 1.0 kcal mol^{-1}. The RMS deviation between the MM parts of structures **I** and **II** is only 0.09 Å, which indicates that hydrogen peroxide binds to the active site without affecting the surrounding protein environment.

1.4.3.2 Formation of Selenenic Acid [E–Se–OH]

In the next stage of the reaction, selenenic acid (E–Se–OH) is formed. As shown previously, the stepwise mechanism consists of two steps: (a) formation of selenolate anion ($E–Se^-$) and (b) O–O bond cleavage.

Formation of Selenolate Anion [$E–Se^-$] In the first step, formation of the selenolate anion ($E–Se^-$) occurs via proton transfer from the Se through the oxygen (O^1) atom of hydrogen peroxide to the neighboring Gln83, leading to intermediate **III** (Figure 1.8). In this process the Gln83 residue plays a role of proton acceptor. This proposal concerning the participation of the Gln83 residue in the reaction is consistent with the available experimental information [20]. The computed barrier for the creation of selenolate anion from structure **II** is 16.4 (12.8) kcal mol^{-1}. However, this value could be slightly overestimated because B3LYP is known to overestimate the activation energy of long-range proton transfer processes [36]. The fully optimized transition state structure [**TS(II-III)**] associated with this barrier is shown in Figure 1.8. As seen from this figure, **TS(II-III)** is stabilized by hydrogen bonds from the Gly50, Gln83, Trp157 and Cso49 residues. In the presence of the surrounding protein, Trp157 forms hydrogen bond with H_2O_2, whereas in the ''active site only'' study Trp157 is hydrogen bonded to Gln83. Compared with the ''active site only'' study, $Gln83H^+–O^1$ and $Se–O^1H$ bond distances are 0.05 and 0.03 Å longer, respectively. This step is calculated to be endothermic by 12.0 (9.5) kcal mol^{-1}. The correction introduced for the different atom types between structures **II** and **III** (in the present case from HS to HO type) reduce the endothermicity by 1.7 kcal mol^{-1}. In intermediate **III**, the O–H bond length in the protonated Gln83 is 1.05 Å, which is 0.03 Å shorter than in the ''active site only'' study. The absence of the active site water molecule slightly increases both barrier and exothermicity by 1.0 and 1.1 kcal mol^{-1}, respectively, in the ''active site only'' calculations. RMS deviations between the MM parts of **II-TS(II-III)** and **II-III** structures are 0.20 and 0.21 Å, respectively.

O–O Bond Cleavage In the second step of the stepwise mechanism, the $O^1–O^2$ bond of H_2O_2 is cleaved. During this process, one hydroxyl fragment (O^1H) is transferred to the selenolate anion [$R–Se^-$] to form selenenic acid [$R–SeO^1H$] while, simultaneously, the second hydroxyl fragment (O^2H) accepts the previously transferred proton from Gln83 to form a water molecule (**IV**, Figure 1.8).

Figure 1.8 shows the optimized transition state [**TS(III-IV)**] for this process. As seen from this figure, all the corresponding distances indicate that this process is synchronous. The calculated barrier for this process is 6.0 (7.6) kcal mol^{-1}. Compared with the ''active site only'' study, the $Se–O^1$ and $Trp157–O^2$ bond distances are 0.11 and 0.43 Å shorter, respectively. Since this step follows the 12.0 kcal mol^{-1} endothermic selenolate anion formation step (from **II** to **III**),

the overall barrier (from **II** to **IV**) for the formation of selenenic acid (E–Se–OH) becomes 18.0 (17.3) kcal mol^{-1}. These results show that the presence of surrounding protein slightly increases the overall barrier by 0.7 kcal mol^{-1}, which is still in a good agreement with the experimentally measured barrier of 14.9 kcal mol^{-1} [21]. Here, it has to be stressed that the active site is not deeply buried inside the enzyme; instead it is located on the interface of two monomers, which is the main reason why the inclusion of protein surroundings does not exert any significant influence on the energetics of the reaction. However, in methane monooxygenase (MMO), cytochrome P450 and triose-phosphate isomerase (TIM) enzymes, where the active sites are deeply buried, the protein surroundings are reported to exhibit considerable effects [37]. The absence of the water molecule at the active site increases the barrier by 2.0 kcal mol^{-1}. This step of the stepwise formation of selenenic acid is calculated to be exothermic by 80.9 (66.6) kcal mol^{-1}. Here, the effect of changing MM atom types (from O_2 to OS) is 1.4 kcal mol^{-1}. RMS deviations between the MM parts of **III-TS(III-IV)** and **III-IV** structures are 0.15 and 0.28 Å, respectively, again indicating that there are no major changes in the protein environment in this step of the mechanism.

Figure 1.9 shows the ONIOM (QM:MM) potential energy diagram for the H_2O_2 reduction mechanism of GPx.

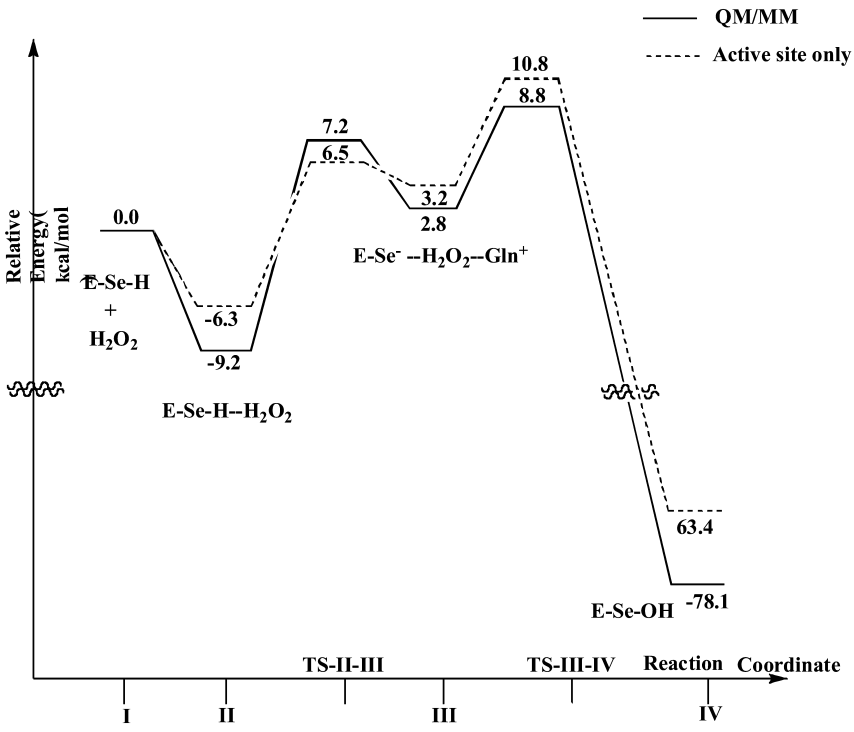

Figure 1.9 Potential energy diagram for the H_2O_2 reduction mechanism of GPx (including solvent effects).

1.4.4
Catalytic Functions: Reductase Activity

The suggested mechanism shown in Figure 1.3 was used as a starting point for this study [38], and for peroxynitrite ($ONOO^-$) and peroxynitrous acid (ONOOH) substrates the overall mechanism is described by the following two reactions, which are calculated to be exothermic by 76.7 (69.9) and 66.4 (62.9) kcal mol^{-1}, respectively:

$$ONOO^- + 2C_2H_5SH \rightarrow C_2H_5S{-}SC_2H_5 + NO_2^- + H_2O \quad (A)$$

$$ONOOH + 2C_2H_5SH \rightarrow C_2H_5S{-}SC_2H_5 + HNO_2 + H_2O \quad (B)$$

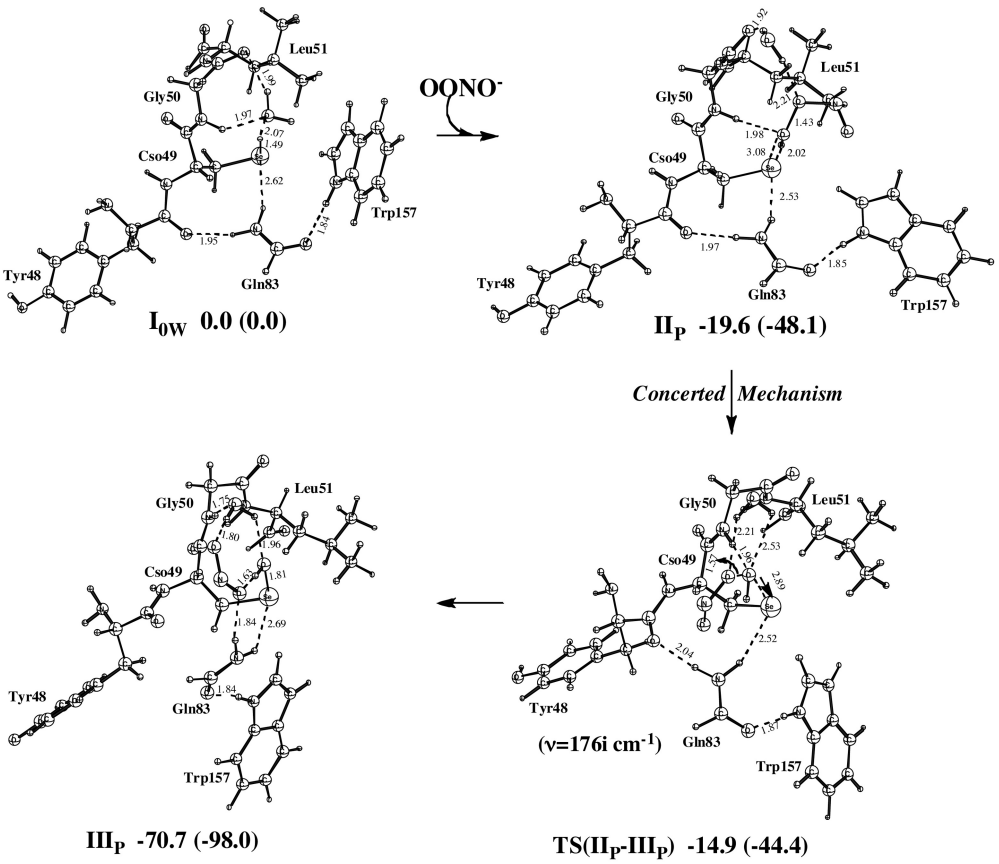

Figure 1.10 Optimized structures (distances in Å) and energies relative to the reactants [with and without (in parenthesis) solvent effects, in kcal mol^{-1}] of intermediates and transition states in Reaction (1) for the concerted "oxidation" mechanism using peroxynitrite ($ONOO^-$) as a substrate.

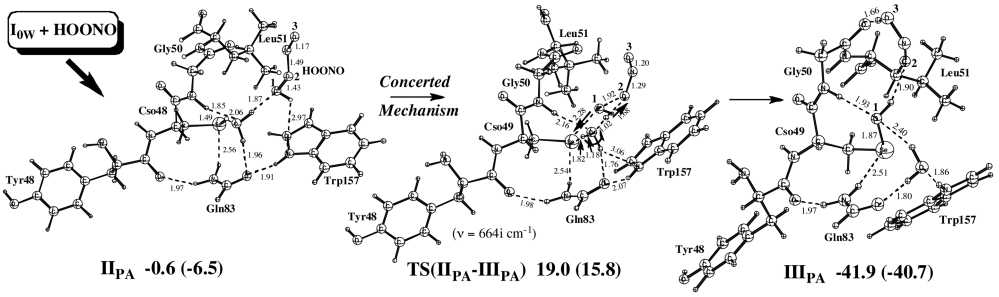

Figure 1.11 Optimized structures (distances in Å) and energies relative to the reactants [with and without (in parenthesis) solvent effects, in kcal mol^{-1}] of intermediates and transition states in Reaction (1) for the concerted "oxidation" mechanism using peroxynitrous acid (ONOOH) as a substrate.

1.4.4.1 Peroxynitrite/Peroxynitrous Acid ($ONOO^-$/ONOOH) Coordination

Coordination of substrate at the active site of GPx enzyme is a first step of both "oxidation" and "nitration" pathways. Coordination of peroxynitrite ($ONOO^-$) to the active site of the enzyme (structure $\mathbf{I_{0W}}$, Figure 1.10) yields structure $\mathbf{II_P}$ ($E–Se^-\cdots HO^1O^2NO^3\cdots H_2O$). $ONOO^-$ acts as a strong base, which abstracts a proton from the E–SeH upon binding to $\mathbf{I_{0W}}$. In $\mathbf{II_P}$, peroxynitrite interacts with the active site through hydrogen bonds with water molecule, selenolate and the Gly50 residue. The binding energy of a free peroxynitrite to $\mathbf{I_{0W}}$ is calculated to be 19.6 (48.1) kcal mol^{-1}.

The protonated form of $ONOO^-$, peroxynitrous acid (ONOOH), binds at the active site of the enzyme (structure $\mathbf{I_{0W}}$) and forms a weakly interacting complex $E–Se–H\cdots H_2O\cdots HO^1O^2NO^3$ (structure $\mathbf{II_{PA}}$, Figure 1.11). The computed binding energy of free peroxynitrous acid is only 0.6 (6.5) kcal mol^{-1}. After the coordination of $ONOO^-$/ONOOH, the catalytic cycle proceeds through the "oxidation" and "nitration" pathways (Figure 1.3), which are discussed separately.

1.4.4.2 Oxidation Pathway

The first process occurring in this pathway is the formation of selenenic acid [E–Se–OH]. The mechanism is quite different for the peroxynitrite and peroxynitrous acid substrates.

Concerted "Oxidation" Mechanism for Peroxynitrite Formation of the oxidation product (E–Se–OH) requires a hydroxyl group. For peroxynitrite ($ONOO^-$), the hydroxyl group required could either be donated by peroxynitrite (now in the form of HOONO in $\mathbf{II_P}$) or a water molecule located near the Se-center. Since the source of the hydroxyl group is not known, both possibilities are explored in this study. In the case where the hydroxyl group is donated by peroxynitrite, the $O^1–O^2$ bond of the previously formed $E–Se^-\cdots HO^1O^2NO^3\cdots H_2O$ complex **($\mathbf{II_P}$)** is broken and the hydroxyl group (O^1H) is concertedly transferred from the substrate to the selenolate ($E–Se^-$) ion to produce $ESe–O^1H$ **($\mathbf{III_P}$)**. The optimized

structure of the corresponding transition state **TS(II_P-III_P)** is shown in Figure 1.10. It is exothermic by 51.1 (49.9) kcal mol^{-1} and proceeds with a barrier of 4.7 (3.7) kcal mol^{-1}. The low barrier for $ONOO^-$ reduction agrees with the experimentally measured barrier of 8.8 kcal mol^{-1} for both GPx and ebselen [23] and the computed value of 7.1 kcal mol^{-1} for ebselen [12]. The removal of a water molecule hydrogen-bonded to $ONOO^-$ from the model makes the peroxynitrite a stronger nucleophile and reduces the barrier by 2.6 (3.3) kcal mol^{-1}. However, notably, this process is most likely to occur in the presence of a water molecule as $ONOO^-$ binding does not remove the water molecule from the active site. The barrier associated with the donation of a hydroxyl group from the water molecule to the $E–Se^-$ is prohibitively high, ca. 40.0 kcal mol^{-1}. These results explicitly indicate that the hydroxyl group required to produce the E–Se–OH is provided by peroxynitrite ($ONOO^-$) that is converted into ONOOH during its coordination. There is no stepwise mechanism corresponding to this step, as the O–O bond cleavage and hydroxyl group transfer are strongly coupled and cannot go through an intermediate.

Concerted "Oxidation" Mechanism for Peroxynitrous Acid For peroxynitrous acid (ONOOH), E–Se–OH formation can take place via either a concerted or a stepwise mechanism. The stepwise mechanism consists of two parts: (a) formation of selenolate anion ($E–Se^-$) and (b) O–O bond cleavage.

In the concerted mechanism for peroxynitrous acid ($O^3NO^2O^1H$), starting from $\mathbf{II_{PA}}$ complex (Figure 1.11), the Se–H bond of the selenol (E–SeH) is broken and, with the help of a bridging water molecule, a proton is transferred to $O^3NO^2O^1H$, which in turn facilitates the $O^1–O^2$ cleavage and, subsequently, the formation of $ESe–O^1H$. Figure 1.11 shows the corresponding transition state **TS(II_{PA}-III_{PA})**. The overall process $\mathbf{II_{PA} \rightarrow III_{PA}}$ is exothermic by 41.3 (34.2) kcal mol^{-1} and proceeds with a 19.6 (22.3) kcal mol^{-1} barrier. In the absence of a water molecule in the model this barrier is further increased by 5.2 kcal mol^{-1} (in the gas phase).

Stepwise "Oxidation" Mechanism for Peroxynitrous Acid In the first step of this mechanism (Figure 1.12) the Se–H bond of the selenol (E–SeH) is broken and, simultaneously, the proton is transferred through the oxygen atom (O^1) of $O^3NO^2O^1H$ and a water molecule to the neighboring Gln83, producing the $\mathbf{II'_{PA}}$ intermediate involving an $E–Se^- + Gln83^+$ ion-pair. The corresponding transition state, **TS(II_{PA}-II'_{PA})**, for this process is stabilized by hydrogen bonds with Gly50 and Trp157 residues. The $\mathbf{II_{PA} \rightarrow II'_{PA}}$ process is endothermic by 5.1 (10.0) kcal mol^{-1} and proceeds with a 6.5 (10.4) kcal mol^{-1} barrier from $\mathbf{II_{PA}}$. In $\mathbf{II'_{PA}}$ the O–H bond (1.08 Å) in $Gln83^+$ is slightly longer than the normal (0.98 Å) O–H bond. The absence of the water molecule in the model increases the barrier (by 6.4 kcal mol^{-1} in the gas phase) and endothermicity (by 6.2 kcal mol^{-1} in the gas phase) of the reaction.

In the second step of the stepwise pathway of E–Se–OH formation, the $O^1–O^2$ bond of $O^3NO^2O^1H$ is cleaved and the hydroxyl (O^1H) is transferred to the sele-

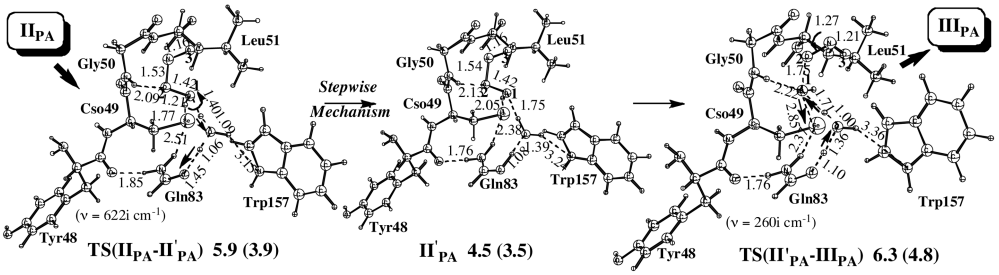

Figure 1.12 Optimized structures (distances in Å) and energies relative to the reactants [with and without (in parenthesis) solvent effects, in kcal mol^{-1}] of intermediates and transition states in Reaction (1) for the stepwise "oxidation" mechanism using peroxynitrous acid (ONOOH) as a substrate.

nolate anion (E–Se$^-$). In this step, the proton previously transferred to the Gln83 residue moves to the oxygen atom (O^2) of $O^3NO^2O^1H$ and initiates the O^1–O^2 bond cleavage. As a result of this process, the E–SeO^1H and HNO_2 (structure **III$_{PA}$**) are produced. The transition state **TS(II′$_{PA}$-III$_{PA}$)** indicates that this step is synchronous, i.e., all bond distances change smoothly from the intermediate **II′$_{PA}$** to the product **III$_{PA}$**. The barrier for this process is only 1.8 (1.3) kcal mol^{-1}, which makes the overall barrier (**II$_{PA}$** → **III$_{PA}$**) for the formation of the selenenic acid (E–Se–OH) 6.9 (11.3) kcal mol^{-1}. The presence of the water molecule significantly stabilizes the transition state as its removal from the model increases the barrier by 13.0 kcal mol^{-1} (gas phase). This step of Reaction (1) is calculated to be exothermic by 46.4 (44.2) kcal mol^{-1}. Since the overall barrier for the stepwise mechanism [6.9 (11.3) kcal mol^{-1}] is substantially lower than the barrier [19.6 (22.3) kcal mol^{-1}] for the concerted mechanism of the E–Se–OH formation, the latter mechanism is ruled out.

The aforementioned results explicitly indicate that the Gln83 residue plays a key role as proton acceptor (step 1) and donor (step 2), which is consistent with the available experimental suggestion that the Gln83 residue participates in the catalytic cycle [20]. Moreover, the water molecule located near the Se-center also plays a very important role by directly participating in the reaction and reducing the barriers. Compared with H_2O_2 reduction by GPx, where the calculated barrier for the enzyme oxidation through the identical stepwise mechanism is reported to be 17.1 (20.6) kcal mol^{-1}, the overall barrier for ONOOH reduction by this enzyme is lower by 10.2 (9.3) kcal mol^{-1}. These results demonstrate that ONOOH is a more efficient substrate for the oxidation of selenocysteine than H_2O_2. In contrast, compared with ebselen (a mimic of GPx), GPx catalyzes the reduction of ONOOH with a barrier higher by 3.9 kcal mol^{-1} (gas phase) [11].

Remaining Steps of the Oxidation Pathway In this pathway, subsequent to the formation of selenenic acid [E–Se–OH], the remaining two steps (Reactions 2 and 3) follow identical mechanisms, as suggested for H_2O_2 reduction by GPx in

our previous computational study [25]. Therefore, these two steps are not discussed here.

1.4.4.3 Nitration Pathways

This pathway, after the binding of $ONOO^-$/ONOOH to the active site (structure $\mathbf{II_{PA}}$), leads to the nitration of the selenol [E–SeH] (Figure 1.13). In general, the nitration product [E–Se–NO_2] can exist in two different isomeric forms, nitro [E–Se–NOO] and nitrito [E–Se–O–N=O], which can be formed by the reactions of both peroxynitrite ($ONOO^-$) and peroxynitrous acid (ONOOH) with the active site selenocysteine residue. However, the use of $ONOO^-$ creates a highly reactive hydroxyl (OH^-) ion that could readily react with the active site amino acid residues. The enzyme may be set-up to control these ions but this unknown regulation process is hard to model. Therefore, to avoid these side reactions, in this study, the ''nitration'' pathway is investigated only for HNOOH substrate. The B3LYP calculations suggest that the formation of the E–Se–NOO (structure $\mathbf{III_{NOO}}$) is thermodynamically, 18.8 (19.0) kcal mol^{-1}, more favorable than the E–Se–O–N=O (structure $\mathbf{III_{ONO}}$), and can occur through the following two

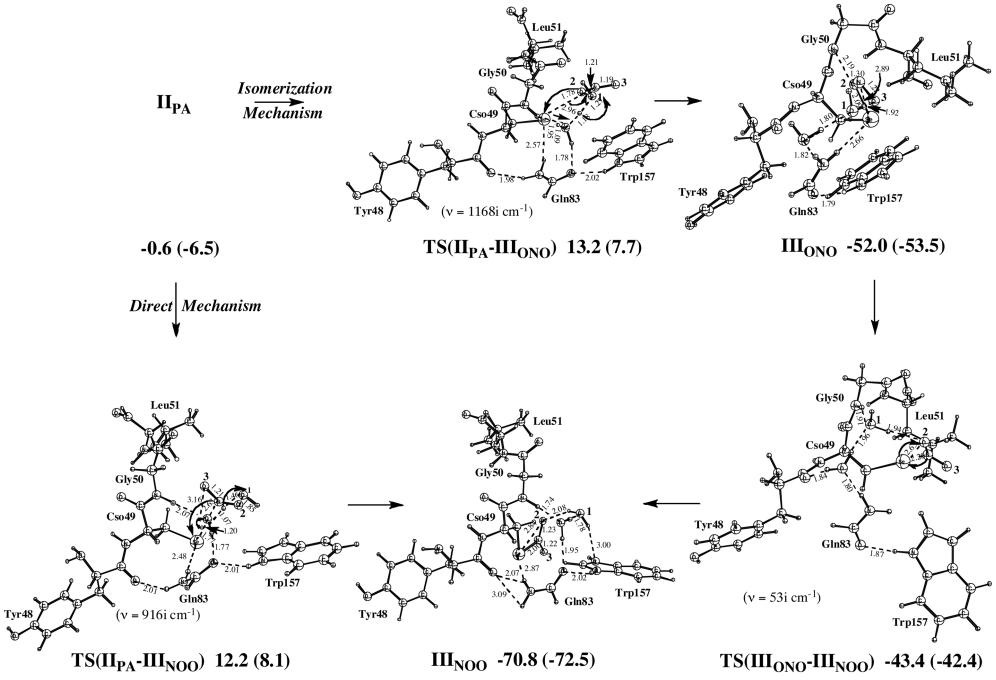

Figure 1.13 Optimized structures (distances in Å) and energies relative to the reactants [with and without (in parenthesis) solvent effects, in kcal mol^{-1}] of intermediates and transition states in Reaction (1) for the isomerization and direct mechanisms in the ''nitration'' pathway using peroxynitrous acid (ONOOH) as a substrate.

mechanisms: (1) isomerization and (2) direct. In the former, the $\mathbf{III_{ONO}}$ species is generated first, which then isomerizes to the energetically more favorable product $\mathbf{III_{NOO}}$, whereas in the latter $\mathbf{III_{NOO}}$ is generated directly.

Isomerization Mechanism In the first part of this mechanism, the Se–H bond of the selenol (E–SeH), $\mathbf{II_{PA}}$, is broken and with the help of the bridging water molecule a proton is transferred to the terminal oxygen atom (O^1) of $O^3NO^2O^1H$, which facilitates O^1–O^2 bond cleavage and leads to the formation of E–Se–O^3–N=O^2 ($\mathbf{III_{ONO}}$) and a water molecule. Figure 1.13 shows the optimized transition state for this process, structure $\mathbf{TS(II_{PA}\text{-}III_{ONO})}$. The computed barrier for the formation of $\mathbf{III_{ONO}}$ is 13.8 (14.2) kcal mol^{-1}, which could be slightly overestimated because the B3LYP method overestimates the activation energy of long-range proton transfer [36]. The formation of this intermediate is exothermic by 51.4 (47.0) kcal mol^{-1}. Similar to the ''oxidation'' pathway, here also the water molecule plays a key role in the mechanism by keeping the barrier low. Removal of the water molecule from the model increases the barrier for this process by 7.2 kcal mol^{-1} (gas phase).

A stepwise mechanism, similar to the one (involving Gln83) investigated for the formation of $\mathbf{III_{PA}}$ in the ''oxidation'' pathway, was also investigated for the generation of $\mathbf{III_{ONO}}$. However, all attempts to locate the transition state for the O^1–O^2 bond splitting of $O^3NO^2O^1H$ failed as its optimization always led to the above discussed concerted mechanism. Based on this result it can be concluded that the stepwise mechanism for the formation of the E–Se–O–N=O product does not exist.

In the second part of this isomerization mechanism, the formed $\mathbf{III_{ONO}}$ isomerizes to $\mathbf{III_{NOO}}$. During this isomerization, the Se–O^2 bond of $\mathbf{III_{ONO}}$ is broken and the Se–N bond is formed. In the associated transition state, $\mathbf{TS(III_{ONO}\text{-}III_{NOO})}$, the Se–$O^2$ and Se–N bond distances of 2.65 and 2.20 Å, respectively, are between the corresponding distances in $\mathbf{III_{ONO}}$ (2.09 and 2.89 Å) and $\mathbf{III_{NOO}}$ (2.84 and 2.00 Å), which clearly indicates the transformation of the intermediate E–Se–O–N=O into E–Se–NOO. $\mathbf{III_{ONO}} \rightarrow \mathbf{III_{NOO}}$ isomerization is found to be exothermic by 18.8 (19.0) kcal mol^{-1} and proceeds with a barrier of 8.6 (11.1) kcal mol^{-1}.

Direct Mechanism In this mechanism, in $\mathbf{II_{PA}}$ the Se–H bond of the selenol (E–SeH) is broken, and with the help of a bridging water molecule a proton is transferred to the terminal oxygen atom (O^1) of $O^3NO^2O^1H$, which in turn cleaves the O^1–O^2 bond and produces the E–Se–NO^2O^3 ($\mathbf{III_{NOO}}$) species and a water molecule (H_2O^1). In the corresponding transition state $\mathbf{TS(II_{PA}\text{-}III_{NOO})}$ (Figure 1.13) the Se–N and Se–O^2 bond distances of 2.63 and 3.16 Å, respectively, clearly indicate the formation of $\mathbf{III_{NOO}}$. The barrier for this concerted mechanism is 12.8 (14.6) kcal mol^{-1} and this process is exothermic by 70.2 (66.0) kcal mol^{-1}. In this process a long-range proton transfer also takes place, which could be slightly overestimated by the B3LYP method [36]. Since for the generation of $\mathbf{III_{ONO}}$ the exclusion of water molecule in the model raises the bar-

rier by 7.2 kcal mol^{-1} (in the gas phase), this possibility is not explored here. As discussed above for the formation of $\mathbf{III_{ONO}}$, the stepwise mechanism involving the Gln83 residue does not exist in the direct generation of $\mathbf{III_{NOO}}$.

The calculated barriers for the nitration of the selenocysteine by peroxynitrous acid through the isomerization and direct mechanisms, 13.8 (14.2) and 12.8 (14.6) kcal mol^{-1}, are very close. While the direct mechanism is slightly preferred, the accuracy of the methods applied in this study does not allow a clear discrimination. Therefore, both these mechanisms for the selenocysteine nitration by ONOOH are plausible.

Reaction of Nitro Product (E–Se–NOO) with Glutathione (GSH) Reaction (2) of the ''nitration'' pathway of Figure 1.3 starts with the coordination of the first unbound glutathione molecule to $\mathbf{III_{NOO}}$ and leads to the formation of a weakly bound (E–SeNO^{2}O^3)–(GSH) complex (**IV**, Figure 1.14) with a binding energy of 1.8 (2.7) kcal mol^{-1}. From **IV** the reaction proceeds through the transition state **TS(IV-V)** and produces the seleno-sulfide (E–Se–S–G) adduct and HNO_2 (structure **V**). As shown in Figure 1.14, at the transition state **TS(IV-V)**, synchronously, the S–H bond of glutathione is broken and, through the water molecule, a proton is transferred to O^3 of the E–Se–NO^{3}O^2 accompanied by the formation of a Se–S bond and nitrous acid (HNO_2). The barrier for this step is calculated to be 9.5 (9.6) kcal mol^{-1} and it is exothermic by 13.9 (12.9) kcal mol^{-1}.

Also in this reaction, the water molecule plays a critical role by significantly reducing the barrier by 15.7 kcal mol^{-1} (in the gas phase). This large effect could be explained by comparing the TS structures with and without the participation of the water molecule. In **TS(IV-V)**, the Se–S and Se–N distances are considerably shorter (0.14 and 0.62 Å, respectively) than the corresponding distances without the water molecule. Moreover, the direct participation of a water molecule also provides an additional hydrogen bond. In the presence of a water molecule **TS(IV-V)** appears to be optimum for the formation of the Se–S bond.

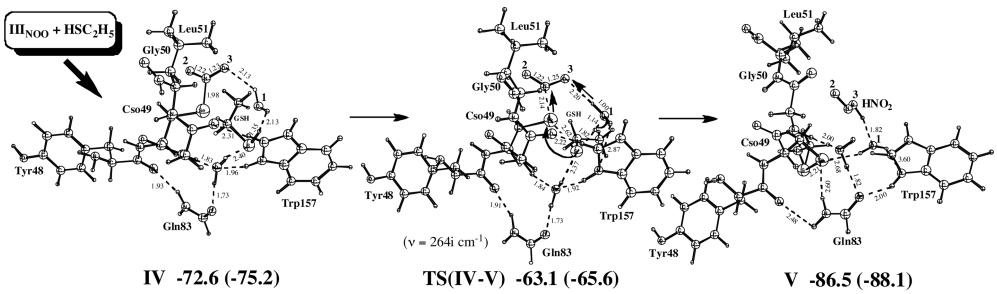

Figure 1.14 Optimized structures (distances in Å) and energies relative to the reactants [with and without (in parenthesis) solvent effects, in kcal mol^{-1}] of intermediates and transition states in Reaction (2) for the ''nitration'' pathway using peroxynitrous acid (ONOOH) as a substrate.

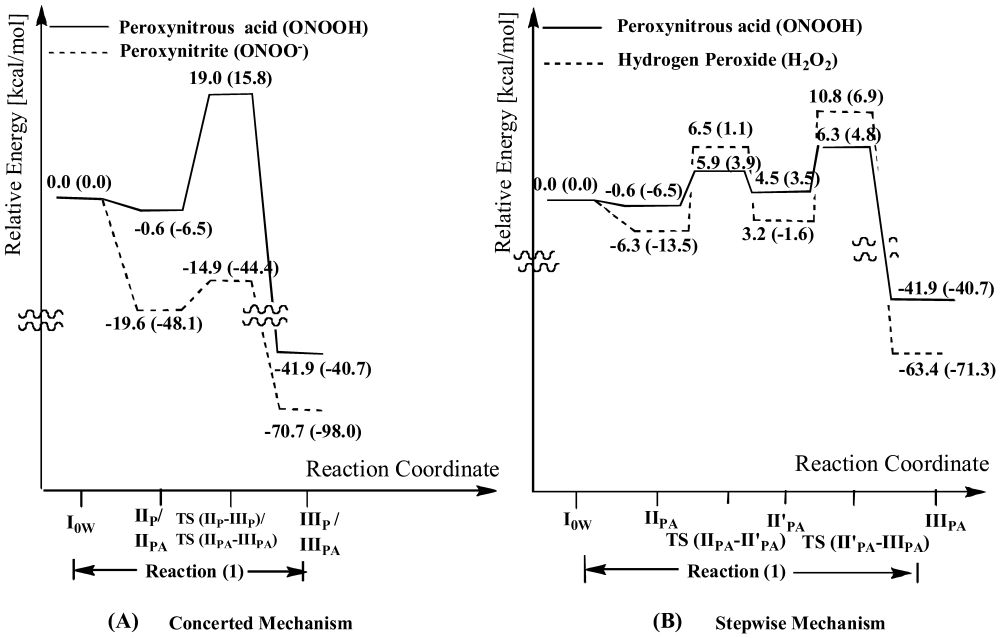

Figure 1.15 (A) Energy diagram for Reaction (1) of the "oxidation" pathway [with and without (in parenthesis) solvent effects, in kcal mol^{-1}]. The energy scale is setup for the values including solvent effects. (B) Energy diagram for reactions (1) and (2) of the "nitration" pathway [with and without (in parenthesis) solvent effects, in kcal mol^{-1}]. The energy scale is setup for the values including solvent effects.

In a similar way, $\mathbf{III_{ONO}}$ is also found to react with the substrate GSH to produce the seleno-sulfide (E–Se–S–G) adduct and HNO_2. First, a molecule of GSH binds to $\mathbf{III_{ONO}}$ to form a $(E–Se–O^3–N=O^2)–(GSH)$ complex (structure $\mathbf{IV_{ONO}}$) with a binding energy of 1.8 (2.7) kcal mol^{-1}, which then rearranges to **V** through $\mathbf{TS(IV_{ONO}\text{-}V)}$ with a small barrier of 1.3 (1.0) kcal mol^{-1}.

After formation of the E–Se–S–G adduct, the third and final step, Reaction (3), of the overall mechanism is identical in both "oxidation" and "nitration" mechanisms (as discussed above). Figure 1.15(A) and (B) shows the overall potential energy diagrams for the concerted and stepwise mechanisms of the "oxidation" pathway.

1.5 Summary

In this chapter we have been explored the structural properties and catalytic functions of the selenoprotein glutathione peroxidase (GPx), utilizing pure quantum mechanics (QM) and hybrid quantum mechanics/molecular mechanics

(QM/MM) approaches. Our discussion is divided into four parts. In the first, the active site of the mammalian GPx is refined using a two-layer ONIOM(QM:MM) method. It was found that the inclusion of two water molecules at the active site provides the lowest root mean square (RMS) deviation from the X-ray structure. Based on these results it was concluded that active site of the enzyme is most likely to have two water molecules. The second part investigated the entire catalytic cycle corresponding to the peroxidase activity of this enzyme, using pure QM (''active site only'') approach. This study reveals important catalytic roles played by Gln83, Gly50 residues and two water molecules. In addition, the generation of the oxidized form of glutathione was proposed to occur with a barrier of 21.5 (25.5) kcal mol^{-1} in the rate-determining step, which is in line with experimental findings. The third part explored the role of the protein surroundings in the mechanism of H_2O_2 reduction, using whole monomer (3113 atoms in 196 amino acid residues), with ONIOM(QM:MM) method. The protein surroundings were calculated to exert a net effect of only 0.70 kcal mol^{-1} (in comparison with the ''active site only'' model) on the overall barrier, which is most likely due to the active site being located at the enzyme surface. The fourth and final part investigated the peroxynitrite reductase activity of GPx at B3LYP level. Our calculations suggest that for peroxynitrite/peroxynitrous acid ($ONOO^-$/ONOOH) substrates the enzyme utilizes two different ''oxidation'' and ''nitration'' pathways. In the ''oxidation'' pathway for $ONOO^-$, the oxidation of GPx and the subsequent formation of the selenenic acid (E–Se–OH) occurs through a concerted mechanism with an energy barrier of 4.7 (3.7) kcal mol^{-1}, which is in good agreement with the computed value of 7.1 kcal mol^{-1} for the drug ebselen and the experimentally measured barrier of 8.8 kcal mol^{-1} for both ebselen and GPx. For ONOOH, formation of the E–Se–OH prefers a stepwise mechanism with an overall barrier of 6.9 (11.3) kcal mol^{-1}, which is 10.2 (11.2) kcal mol^{-1} lower than that for hydrogen peroxide (H_2O_2), indicating that ONOOH is a more efficient substrate for GPx oxidation. The nitration of GPx by ONOOH produces a nitro (E–Se–NO_2) product via either of two different mechanisms, isomerization and direct, having almost the same barrier heights. Comparison of the rate-determining barriers of the ''oxidation'' and ''nitration'' pathways suggests that the oxidation of GPx by ONOOH is more preferable than its nitration. It was also shown that the rate-determining barriers remain the same, 21.5 (25.5) kcal mol^{-1}, in the peroxynitrite reductase and peroxidase activities of GPx.

References

1 Combs, G. F. Jr., Lü, J., *Selenium Its Molecular Biology and Role in Human Health*, ed. D. L. Hatfield, Kluwer Academic Publishers, Boston, 2001, p. 205.

2 Zhao, L., Cox, A. G., Ruzicka, J. A., Bhat, A. A., Zhang, W., Taylor, E. W. *Proc. Natl. Acad. Sci. U.S.A.* 2000, **97**, 6356.

3 Birringer, M., Pilawa, S., Flohè, L. Trends in selenium Chemistry, *Nat. Prod. Rep.* 2002, **19**, 693–718.

4 Mills, G. C. *J. Biol. Chem.* 1957, **229**, 189–197.
5 Flohè, L., *Glutathione*, eds. Dolphin, D., Avramovic, O., Poulson R., John Wiley & Sons, New York, 1989, pp. 644–731.
6 Sies, H., Sharov, V. S., Klotz, L. O., Briviba, K. *J. Biol. Chem.* 1997, **272**, 27812–27817.
7 Björnstedt, M., Xue, J., Huang, W., Akesson, B., Holmgren, A. *J. Biol. Chem.* 1994, **269**, 29382.
8 Godeas, C., Sandri, G., Panfili, E. *Biochim. Biophys. Acta* 1994, **1191**, 147.
9 Roveri, A., Ursini, F., Flohé, L., Maiorino, M. *Biofactors* 2001, **14**, 213.
10 Sies, H., Masumoto, H. *Adv. Pharmacol.* 1997, **38**, 229–246.
11 Musaev, D. G., Hirao, K. *J. Phys. Chem. A* 2003, **107**, 9984–9990.
12 Musaev, D. G., Geletii, Y. V., Hill, C. L., Hirao, K. *J. Am. Chem. Soc.* 2003, **125**, 3877–3888.
13 Epp, O., Ladenstein, R., Wendel, A. *Eur. J. Biochem.* 1983, **133**, 51–69.
14 Ren, B., Huang, W., Åkesson, B., Ladenstein, R. *J. Mol. Biol.* 1997, **268**, 869–885.
15 Prohaska, J. R., Oh, S. H., Hoekstra, W. G., Ganther, H. E. *Biochem. Biophys. Res. Commun.* 1977, **74**, 64–71.
16 Forstrom, J. W., Zakowski, J. J., Tappel, A. L. *Biochemistry* 1978, **17**, 2639–2644.
17 Wendel, A., Pilz, W., Ladenstein, R., Sawatzki, G., Weser, U. *Biochim. Biophys. Acta* 1975, **377**, 211–215.
18 Ladenstein, R., Epp, O., Bartels, K., Jones, A., Huber, R., Wendel, A. *J. Mol. Biol.* 1979, **134**, 199–218.
19 Kraus, R. J., Ganther, H. E. *Biochem. Biophys. Res. Commun.* 1980, **96**, 1116–1122.
20 Ursini, F., Maiorino, M., Brigelius-Flohé, R., Aumann, K. D., Roveri, A., Schomburg, D., Flohé, L. *Methods Enzymol.* 1995, **252**, 38–53.
21 Roy, G., Nethaji, M., Mugesh, G. *J. Am. Chem. Soc.* 2004, **126**, 2712–2713.
22 Mugesh, G., du Mont, W., Sies, H. *Chem. Rev.* 2001, **101**, 2125–2179.
23 Briviba, K., Kissner, R., Koppenol, W. H., Sies, H. *Chem. Res. Toxicol.* 1998, **11**, 1398–1401.
24 Padmaja, S., Squadrito, G. L., Pryor, W. A. *Arch. Biochem. Biophys.* 1998, **349**, 1–6.
25 Prabhakar, R., Vreven, T., Morokuma, K., Musaev, D. G. *Biochemistry* 2005, **44**, 11864–11871.
26 *Gaussian 03 (Revision C1)*, Frisch, M. J. et al. (2004) Gaussian Inc., Pittsburgh, PA.
27 (a) Becke, A. D. *Phys. Rev. A* 1988, **38**, 3098–3100. (b) Lee, C., Yang, W., Parr, R. G. *Phys. Rev. B* 1988, **37**, 785–789. (c) Becke, A. D. *J. Chem Phys* 1993, **98**, 5648–5652.
28 Siegbahn, P. E. M., Blomberg, M. R. A. *Chem. Rev.* 2000, **100**, 421–437.
29 Cances, E., Mennucci, B., Tomasi, J. *J. Chem. Phys.* 1997, **107**, 3032–3041.
30 Maseras, F., Morokuma, K. *J. Comp. Chem.* 1995, **16**, 1170–1179.
31 Dapprich, S., Komaromi, I., Byun, S., Morokuma, K., Frisch, M. J. *J. Mol. Struct. (Theochem)* 1999, **461**, 1–23.
32 Bakowies, D., Thiel, W. *J. Phys. Chem.* 1996, **100**, 10580.
33 *GaussianView 3.0*, Gaussian Inc., Pittsburgh, PA, 2003.
34 Prabhakar, R., Musaev, D. G., Khavrutskii, I. V., Morokuma, K. *J. Phys. Chem. B* 2004, **108**, 12643–12645.
35 Prabhakar, R., Vreven, T., Morokuma, K., Musaev, D. G. *J. Phys. Chem. B* 2006, **110**, 13608–13613.
36 Prabhakar, R., Blomberg, M. R. A., Siegbahn, P. E. M. *Theor. Chem. Acc.* 2000, **104**, 461–470.
37 Friesner, R. A., Gullar, V. *Annu. Rev. Phys. Chem.* 2005, **56**, 389–427.
38 Prabhakar, R., Vreven, T., Morokuma, K., Musaev, D. G. *Biochemistry* 2006, **45**, 6967–6977.